PCCP

PAPER

Cite this: *Phys. Chem. Chem. Phys.*, 2018, **20**, 16625

Effect of UV radiation damage in air on polymer film thickness, studied by soft X-ray spectromicroscopy†

Lis G. A. Melo,*[a] Adam P. Hitchcock,[a] Darija Susac,[b] Juergen Stumper[b] and Viatcheslav Berejnov[b]

Received 25th December 2017, Accepted 27th May 2018

DOI: 10.1039/c7cp08621k

rsc.li/pccp

The thicknesses of thin films of polystyrene (PS), poly(methyl methacrylate) (PMMA), and perfluorosulfonic acid (PFSA) were measured by Ultraviolet Spectral Reflectance (UV-SR) and Scanning Transmission X-ray Microscopy (STXM). At high doses, the UV irradiation in air used in the UV-SR method was found to modify the chemical structures of PS and PMMA (but not PFSA), leading to thinning of these polymer films. The chemical changes caused by UV/air radiation damage were characterized by STXM. When UV and X-ray radiation are applied using no-damage conditions, the film thicknesses measured with the two techniques differ by less than 15% for PS and PMMA and less than 5% for PFSA. This is an important result for verifying the quantitation capabilities of STXM. The chemical damage to PS and PMMA is explained by oxygen implantation from air with formation of ozone. The thickness depletion caused by UV/air radiation for PS and PMMA films is exponential with exposure time. Different rates of depletion are linked to surface or bulk driven photo-chemical product erosion. The initial rate of material erosion was found to be constant and non-specific to the studied polymers.

Introduction

Accurate measurements of the thickness of polymer thin films in the range of 20–500 nm with a few percent precision are important in many fields including lithography, organic electronics, fuel cells and Li-batteries. Depending on the application, the polymeric material could be either deposited on a flat substrate (*e.g.* for lithography and organic electronics) or distributed in a porous structure such as within the catalyst layer (CL) electrode in polymer electrolyte membrane fuel cells (PEM-FC). An important aspect of PEM-FC catalyst layer characterization is the determination of the amounts and spatial distributions of the major CL components – ionomer, carbon support and Pt catalyst. Scanning transmission soft X-ray microscopy (STXM) has been used to map the effective thickness of the perfluorosulfonic acid (PFSA) ionomer dispersed in CL.[1,2] The STXM thickness measurements are based on the analysis of component specific X-ray absorption.[3,4] The quantity of a particular component can be deduced from its effective thickness, the portion of a given volume that component occupies in the CL. If accurate measurements of the effective thickness can be made, then more precise structure–property-performance correlations can be achieved and used to improve manufacturing processes to optimize CL properties. The accuracy of STXM-based thickness determination has not been documented previously to our knowledge.

The thickness of chemically homogeneous and uniformly thick films can be measured with a variety of methods, including atomic force microscopy,[5,6] optical profilometry,[7,8] reflectometry,[9,10] ellipsometry[11–15] and Ultraviolet Spectral Reflectance[16–22] (UV-SR).‡ The optical methods are direct, provide absolute thicknesses, and give an average value over a sample area in the micron range. They are usually fast and very convenient for industrial application where it is often critical to monitor film thickness over large areas.

However, optical techniques are not suitable for the analysis of polymer thickness in porous systems. For that reason, the ability of STXM to measure the effective ionomer thickness across the CL is very unique. In the context of establishing a robust analytical method, it is important to evaluate the accuracy of the STXM effective thickness measurement. This can be done by comparing STXM derived thicknesses with results from another independent method applied to the same sample.

[a] Dept. Chemistry and Chemical Biology, McMaster University, Hamilton, ON L8S 4M1, Canada. E-mail: lismellow@gmail.com

[b] Automotive Fuel Cell Corporation Corp., 9000 Glenlyon Parkway, Burnaby, BC, V5J 5J8, Canada

† Electronic supplementary information (ESI) available: Supplementary figures and tables. See DOI: 10.1039/c7cp08621k

‡ While SR is often used as the acronym for spectral reflectance we choose to use UV-SR in this paper to avoid confusion with the common use in the X-ray microscopy community of SR for synchrotron radiation.

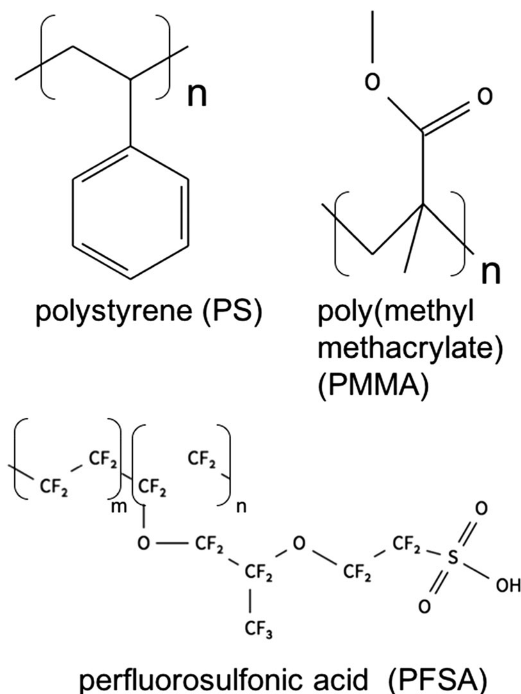

Scheme 1 Chemical structures of polystyrene (PS), polymethylmethacrylate (PMMA), perfluorosulfonic acid (PFSA), equivalent weight (EW) = 1100, where $m/n \sim 6$.

Therefore, the main objective of this study is to evaluate the accuracy of STXM thickness measurements by correlating STXM results with those obtained from UV-SR. For this work, spun-cast homogeneous thin films of three polymers were used: polystyrene (PS), poly(methyl methacrylate) (PMMA) and perfluorosulfonic acid (PFSA) (Scheme 1). A commercial UV-SR instrument, a Filmetrics model F40-UV,[23] which performs thin film thickness measurements based on the analysis of the interference response in a wide range of photon wavelengths from UV to infrared, was used in this work. By confirming the accuracy of STXM thickness determination for several different types of homogeneous thin films, the confidence in results measured from porous CL systems is increased. It was found that if the UV and X-ray measurements were performed under low dose conditions that do not result in chemical changes, then the thicknesses of films in the 30–200 nm range measured with both techniques differ by $<10\%$. This is first direct, independent verification of the accuracy of STXM thickness determination. This is important since X-ray absorption derives thickness values based on mass and identity of the absorptive material, while UV-SR derives thickness from optical interference which is related to photon wavelength.

It is known that both the soft X-ray irradiation in He used in STXM and the UV irradiation in air used for UV-SR can induce chemical changes in polymer materials.[24–30] Therefore, thickness measurements acceptable for instrument cross-correlation must be conducted using optimized conditions which are known not to produce chemical alterations. In carrying out measurements to define low damage conditions, we found that PS and PMMA films are extensively modified for UV/air exposure times >2 min. Moreover, if the exposure time increases to 5 min or more in the same area, which is the case when one is looking to increase the precision of the measurement or when creating thickness maps, both the film thickness and optical constants change, bringing into question the accuracy of UV-SR measurements. In order to understand these effects, we used near edge X-ray absorption fine structure (NEXAFS) spectroscopy in STXM to characterize the chemical changes to PS and PMMA films caused by UV/air irradiation. In contrast to PS and PMMA, the thickness of PFSA measured by UV-SR was constant over a large range of exposure times indicating PFSA is not damaged by UV/air irradiation. The chemical change of polymers measured by NEXAFS caused by UV/air radiation damage is explained by assuming oxygen implantation into the film from air with simultaneous formation of ozone in close proximity of the film/air interface. The mathematic model of thickness depletion due to UV/air radiation for PS and PMMA films is presented as an exponential behavior with the exposure time. The model outputs different rates of depletion depending on the type of polymer and is linked to either surface or bulk driven erosion of photo-chemical products. The initial rate of material erosion corresponding to small thickness depletion was found to be constant and similar for both PS and PMMA polymers.

Experimental methods

Sample preparation

Polystyrene (molecular weight (MW) = 344 kD) was obtained from Polymer Source Inc. PMMA (MW = 120 kD) was obtained from Sigma Aldrich. A PFSA alcohol-based dispersion with the commercial name of Dupont D521Nafion® was obtained from Ion Power. PS and PMMA were diluted with toluene (99.5%) obtained from Anachemia. For spin coating, the PFSA dispersion was further diluted with isopropyl alcohol (IPA) to between 1 and 3% (wt/wt) depending on the desired thickness. 0.5 to 1 g solutions of each polymer were prepared fresh for each use. Ultrasonication at 50 °C for 15 min was used to ensure the polymers were completely dissolved.[31]

The solutions were spin-coated on a cleaved mica substrate. A Specialty Coating Systems model 6708D spin coater was used. After spin-coating, the mica surface with the polymer film was cut into 1 mm^2 squares with a clean scalpel blade. The polymer film was then lifted off the substrate by immersing the sample into a distilled water bath. A floating piece of film was then transferred onto the top surface of a SiNx window. The SiNx windows, which were 75 nm thick with 2×2 mm membrane area in a 5×5 mm, 0.2 mm thick Si wafer frame, were obtained from Norcada Inc.

UV spectral reflectance (UV-SR)

The UV spectral reflectance method is based on the interference of incident light beams in the UV to IR regions (190–2200 nm) with part of those beams reflected from the air/material and material/substrate interfaces (see Fig. 1a).[23] The interference pattern depends on the light wavelength, λ, the film thickness,

 This journal is © the Owner Societies 2018

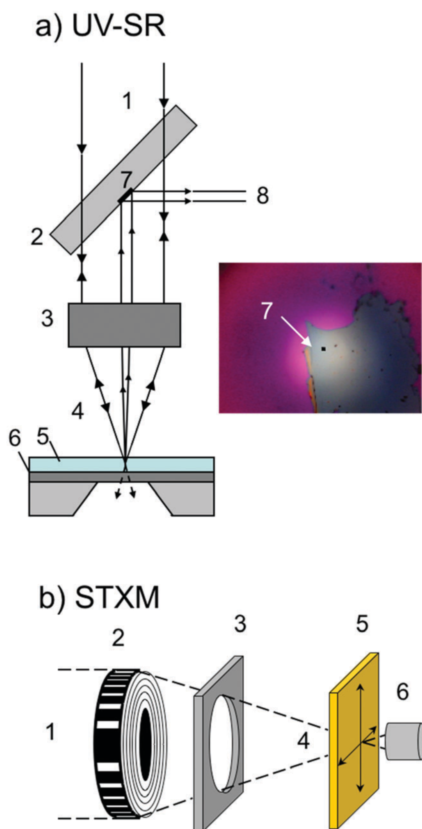

Fig. 1 (a) Schematic of UV spectral reflectance (UV-SR): 1 – incident beam, 2 – beam splitter, 3 – objective lenses, 4 – incident and sample reflected beams, 5 – thin film of PS on SiNx/Si, 6 – SiNx window substrate on a Si wafer, 7 – mirror (pin hole, also called the probe area), 8 – beam directed to spectrometer. Inset shows size of the signal acquisition area, mirror 7 compared to the total illuminated spot of ~500 μm diameter. (b) Schematic of scanning transmission X-ray microscopy (STXM): 1 – monochromated soft X-rays from the beamline, 2 – zone plate, 3 – order sorting aperture, 4 – first order diffracted soft X-ray beam, 5 – sample raster scanned in X and Y directions orthogonal to the beam, 6 – detector.

h, and the optical properties of the material and therefore its refractive index, n, which is also a function of the wavelength. The spectrum of the reflected light, $R(\lambda)$, contains interference fringes with a wavelength and thickness dependence which is described *qualitatively* by:

$$R(\lambda) = A + B\cos(4\pi \times h \times n(\lambda)/\lambda) \quad (1)$$

where A and B are complex functions incorporating the extinction coefficient, $k(\lambda)$, and the refractive index, $n(\lambda)$. Together k and n are called the "optical constants of the material" in this work.[23,32] The experimental $R(\lambda)$ spectrum is then fit to a theoretical model. In this study, all data in the interval of $250 < \lambda < 1000$ nm were fit using the "amorphous model", a proprietary model of Filmetrics.[23]

The polymer film mounted on the SiNx window covers the thin SiNx membrane in areas with and without the underlying Si frame. The part of the polymer film deposited on the window area (*i.e.* without underlying Si) was used for STXM and UV-SR correlation measurements. This allows measurements by both instruments on areas of the polymer films which are at the same position within a few tens of microns (see Fig. S1 and S1, ESI†). UV-SR imaging experiments indicate the films were uniform to within 3% over these dimensions, with no evident structure on the few micron scale. The deposited polymer film on the SiNx membrane backed by a reflecting Si surface was used for those cases where only UV-SR measurements were made. The optical constants of the SiNx membrane were determined by UV-SR for each sample. The SiNx refractive indices measured at 630 nm were in the range of (2.168–2.219), depending on the window batch. These values differ from the range of 2.15–2.17 reported by Norcada,[33] as low stress silicon nitride thin membranes are non-stoichiometric silicon oxy-nitride.

Two methods of analysis of the UV-SR results were used: (i) based on measured optical constants, and (ii) based on assumption of applicability of previously measured optical constants. Method-i requires films thicker than 50 nm which can develop several interference fringes for the $R(\lambda)$ spectrum in order to accurately determine several parameters simultaneously. Method-ii has only a single parameter so that even a part of the interference fringe in the $R(\lambda)$ spectrum is enough to determine thickness. Upon UV/air exposure, radiation damage may change both the optical constants and film thickness. This effect is explored in a following section by comparing the thickness determined when the optical constants are assumed to be unchanged (method-ii) to that determined when optical constants were measured for each exposure (method-i).

UV-SR was measured using a Filmetrics model F-40UV, equipped with objective lenses, light source (model LS-DT2), spectrometer with a wavelength interval of $190 < \lambda < 1100$ nm§ and the StageBase-XY10-Auto motion stage. Fig. 1a describes the F-40UV instrument. The ~500 μm diameter optical probe directed normal to the sample film (5) is provided by two sources (1, 4), a deuterium lamp (UV) with output over $190 < \lambda < 400$ nm wavelengths, and a halogen white light lamp with output over $380 < \lambda < 2200$ nm. The polymer sample receives the polychromatic light through a fiber optic, which conducts the light from the two sources through the objective lens to the sample. The low wavelength cutoff of the fiber optic used is ~250 nm, which defines the lowest UV wavelength received by the sample and passed to the spectrometer. For imaging, a 15× UV compatible objective lens (3) was used, providing a field of view of ~500 μm diameter at the sample plane. The signal for $R(\lambda)$ measurements was taken from a much smaller area (7), 7 × 7 μm in the center of the field of view, with an optimally focused sample. The reflected light from this probe area is redirected into the spectrometer (8). For this model Filmetrics claims a refractive index accuracy of 0.2% for determining film thicknesses (5) in the range 4 nm to 10 μm.[23] Radiation intensity specifications for the light sources were not provided by Filmetrics. Background measurements without the sample were taken every 30 min and used over time intervals no longer than one hour. All measurements were done in a laboratory ambient

§ The Filmetrics model F40UV light sources provide radiation from $190 < \lambda < 2200$. However, the fibre optic used to transport the light has a low wavelength cut-off of 250 nm.

environment with controlled temperature (T is 20 to 22 °C) and relative humidity (RH is 40 to 50%).

Scanning transmission X-ray microscopy (STXM)

STXM[34,35] is a synchrotron-based technique that forms images by raster scanning the sample through a focused, monochromatic X-ray beam, shown in Fig. 1b. Measurements were performed using the ambient STXM at the 10ID1 spectromicroscopy beam line[36] at the Canadian Light Source (CLS) and at the polymer STXM[37] on beamline 5.3.2.2[38] at the Advanced Light Source (ALS). The monochromated soft X-ray beam (1) illuminates a Fresnel zone plate (2) (provided by the Centre for X-ray Optics, Berkeley Lab) which focuses part of the X-rays to a spot size of $\sim$30 nm at the sample (5). The first order diffracted X-rays (4) are isolated from the unfocused X-rays by an order selected aperture (3) and the central stop of the zone plate. The sample is raster scanned in X and Y while the transmitted X-ray intensity is measured by a phosphor/photomultiplier detector (6), producing a transmission image.[3,34,37] The high chemical contrast in STXM images arises from material specific X-ray absorption at different photon energies.[39] The measured transmitted intensity at each pixel is converted to optical density, OD, using the Lambert–Beer law:

$$\mathrm{OD}(E) = -\ln(I(E)/I_0(E)) \quad (2)$$

where $I(E)$ is the intensity transmitted through the sample and $I_0(E)$ is the intensity of the incident photon beam at photon energy E. If the material in the probe area is composed of multiple chemical species (components), the measured OD is a linear combination of absorption of all components:

$$\mathrm{OD}(E) = \sum_i \mathrm{OD1}(E)_i h_i \quad (3)$$

where $\mathrm{OD1}(E)_i$ is the reference spectrum of component i obtained from experiment, and h_i is the effective thickness of component i. Reference spectra were obtained for each pure component which were set on an absolute $\mathrm{OD1}(E)_i$ intensity scale of optical density per 1 nm thickness[34] by scaling the measured spectrum of the pure component outside of the near edge region to the spectrum of the component mass absorption coefficient $\mu_i(E)$.[40] See ESI,† S2 for further details on this procedure.

The STXM data was analyzed using aXis2000 software.[41] Image sequences or stacks[42] were recorded at specific edges (C 1s, O 1s, F 1s). In order to minimize the radiation damage from soft X-ray exposure (which is known to occur at quite low doses for PMMA[25,27] and PFSA[43]), all stacks were measured under negligible X-ray damage conditions, with exit slit sizes set to limit the incident photon intensity to $<$5 MHz, the X-ray beam defocused to a diameter of 500–700 nm, a pixel spacing of the same size as the defocused spot size, and a dwell time of 1 ms per pixel. The signal from areas between 900–2000 μm^2 was measured in several regions in all three materials (PS, PMMA and PFSA). In order to verify that these conditions did not cause X-ray damage, after the stack was completed an image was recorded over an area larger than the area of the stack, at the photon energy of highest X-ray damage contrast (285.2 eV for PS, 288.4 eV for PMMA and 292.4 eV for PFSA). There was no change in the OD values between the stack areas and adjacent non-irradiated areas for any of the materials studied. This means that the conditions used did not cause any radiation damage detectable by STXM, so STXM can be used to detect spectral changes in the UV-SR exposed sample areas without itself making any chemical modifications to the polymer film.

The accuracy of the STXM thickness determination was improved by measuring the same area at several edges *i.e.* C 1s for all 3 polymers, O 1s for PMMA and F 1s for PFSA. The stacks were appended and aligned together. I_0 was recorded for each Y line of pixels of the image and used to convert the transmitted intensity to optical density. The OD(E) spectrum was averaged over the entire available probe area, excluding defects irrelevant to the single layer of the polymer film *i.e.* dust particles, folds, and the edge of the film. The OD(E) spectrum was then divided by the OD1(E) reference spectrum for that particular polymer to get an effective thickness h = OD(E)/OD1(E), hereafter just labeled thickness. Based on repetitive measurements at the combined edges (three regions in a thick sample and three regions in a thin sample of each material), there were 6 sets of thickness values for PS (280 data points/edge) and PMMA (264 data points/edge) and 4 sets for PFSA (380 data points/edge). This numerical data was further analyzed using Excel to find the average, standard deviation and standard error for the thicknesses of each material.

Characterizing material sensitivity to UV exposure

The Filmetrics F40-UV instrument focuses the light to a spot of $\sim$500 μm diameter on the sample. However, the UV-SR spectrometer only reads the reflected signal from $\sim$50 μm^2 (see Fig. 1a, label 7) thus providing only one thickness data point while STXM measures $\sim$30 spots of 0.5–0.7 μm each. To determine whether the UV-SR thickness results were affected by possible UV radiation damage occurring during measurements, the thickness of each sample was measured at two characteristic time intervals: (i) short – sufficient for the measurement to produce adequate signal-to-noise ratio, and (ii) long – sufficient to observe material changes. The short intervals (up to 2 min total exposure) were used for quantitative measurements to compare to STXM results on the same area. The long exposures were performed by continuously exposing the same area for up to 30 min or 60 min at a fixed irradiation rate (unknown for UV-SR, but always constant) and then performing the UV-SR thickness measurement which takes $\sim$5 s at specific time points during that long exposure. If the material is not affected by the UV/air irradiation, then one can assume the thickness and optical constants should not change. In the case of radiation damage, these values are expected to change systematically with exposure time. A similar method using different regions for each dose is well established for STXM,[25,44] but this type of systematic exposure dependence has not been applied previously to UV-SR to the best of our knowledge.

The UV-SR conditions for providing minimal radiation damage were: UV-lamp warm-up time $\sim$15 min; total measurement

time <30 to 40 s including finding the region of interest, focusing, and taking repetitive reflectivity measurements if needed. The maximum time interval available for thickness measurements before the UV radiation damage is detectable was estimated from plots of the thickness *versus* exposure time and extrapolated to zero exposure time to obtain the non-damaged thickness. For PMMA and PS the no-damage interval is <2 min. When comparing polymer film thicknesses determined by UV-SR and STXM, the same area of the film on a SiNx window was measured by UV-SR in <2 min, and by STXM using no-damage conditions.

Repeat measurements were made in order to characterize the measurement uncertainty and find the standard error and standard deviation for each technique. For UV-SR, this was done for two instances: (i) in a pristine area of the sample not previously exposed to any radiation, and (ii) for regions of the sample previously exposed to UV light (*e.g.* the 30 min exposure under the UV-SR light source), after STXM analysis. In each case, the UV-SR measurements were repeated in the same area for each material for up to a total of 13 measurements involving ∼60–100 s of UV exposure time (see Table 1 for details of the replicate measurements).

Results

UV-SR: effect of UV exposure on film thickness

Upper limit of UV exposure time for reliable thickness measurements. Fig. 2 plots the thicknesses of PS, PMMA and PFSA spun cast films and a SiNx film on a Si wafer, measured by UV-SR as a function of the time the same spot was exposed to UV/air. The thicknesses reported in Fig. 2 were evaluated using the same optical constants (method-ii) for all exposure times. The initial thicknesses of the PMMA, PFSA, PS and SiNx thin films, determined by UV-SR with low UV exposure conditions, were 33, 52, 41 and 67 nm, respectively. The different material sensitivity to the UV/air irradiation is apparent: PMMA and PS suffer extensive thickness reduction as the exposure time increases, while PFSA and the SiNx substrate are unaffected by the UV exposure. For PMMA and PS an exposure of 2.0 min

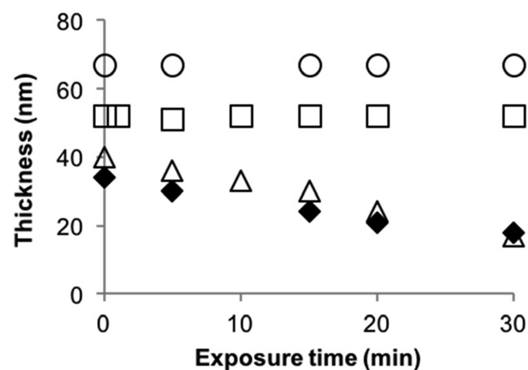

Fig. 2 Absolute thickness (nm) of thin films of silicon nitride (SiNx); and PS, PMMA and PFSA thin films on a SiNx window, measured by UV-SR at 0, 5, 10, 15, 20, and 30 min exposure time in air. □ = PFSA on SiNx; ♦ = PMMA on SiNx; Δ = PS on SiNx; O = SiNx.

and 1.5 min causes a thickness change of 1 nm which is 3% and 2.5% of the film thickness, respectively. These results set an upper bound of exposure times for obtaining meaningful thicknesses for the original PMMA and PS films when using Filmetrics UV-SR in a laboratory environment. The thicknesses of SiNx and PFSA are constant over 30 min UV exposure, within the measurement uncertainty (±1 nm).

Sensitivity of Filmetrics fitting procedure to extent of UV/air exposure. The Filmetrics instrument determines film thickness from a fit of a specific optical model to the $R(\lambda)$ spectrum. The quality of the fit depends on how many interference fringes are developed by the measured area of a particular film. We expect that UV radiation damage changes both the thickness (as documented in Fig. 2) and the optical constants. Below we show how this affects the fitting procedure and thus the derived results.

In order to test the sensitivity of the Filmetrics fitting to changes caused by the UV exposure, UV-SR measurements were made for two different initial thicknesses of PMMA: 92 and 49 nm (results presented in Fig. 3) and for PS: 110 and 49 nm (results presented in Fig. 4). The same method and exposure conditions were used to measure all four samples. The polymer films were deposited on a SiNx film on top of the 0.2 mm Si wafer frame. To test the sensitivity of the fitting procedure for

Table 1 UV-SR thickness as a function of total UV-SR measurement time for multiple areas of PS and PMMA thin films on SiNx to calculate the standard deviation

		PS					PMMA				
Sample[a]		$[\,]^b$ wt%	Total time[c] (s)	#[f]	Thickness (nm)	Std dev	$[\,]^b$ wt%	Total time[c] (s)	#[f]	Thickness (nm)	Std dev
Pristine	I	2	65	7	122.6	0.5	3[e]	75	9	96.4	0.8
	II	1	90	12	43.5	0.2	3[e]	55	5	73.7	0.8
	III	—	—	—	—	—	1.5	85	11	47.7	0.7
Damaged[d]	I	2	85	11	79.6	0.6	3[e]	85	11	39.7	0.8
	II	1	90	12	35.3	0.4	3[e]	85	11	27.4	1.0
	III	—	—	—	—	—	1.5	75	9	24.5	1.2

[a] Samples I, II and III are distinct samples, made with different solution concentrations, except for the replicate PMMA 3% samples – see footnote (e). [b] Concentration of spin coat sample (wt% in toluene). [c] The exposure time for generating the damage is not counted towards the exposure time for determining the reproducibility of the measurements. [d] Damaged areas were exposed to the UV-SR for 30 to 60 min, depending on initial thickness. [e] Samples I and II are separate samples made from the same solution. [f] Number of measurements taken for the same area to get the thickness average and standard deviation.

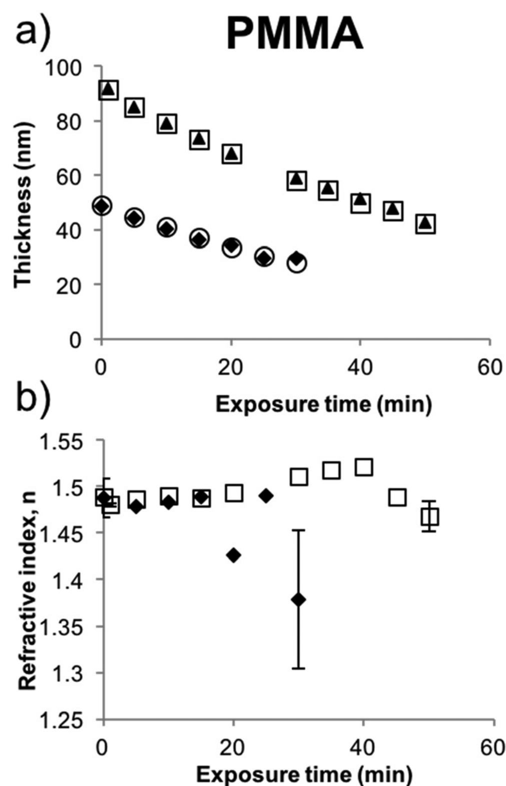

Fig. 3 Effect of UV/air exposure time (min) on PMMA: (a) thickness (nm) and (b) refractive index values, determined by UV-SR for two samples of PMMA on a SiNx window (on the Si frame) with initial thicknesses of 49 nm and 91 nm. ○ = thin(t) and ▲ = thick(t) are values where only the thickness was determined using method-ii with k = 0 and fixed refractive index of 1.482 ± 0.001 at λ = 632.8 nm. ♦ = thin(t,n,k) and □ = thick(t,n,k) are values where both thickness and optical constants were determined using method-i. Note that the larger error bar at the 30 min exposure is because the thickness has decreased to values where the signal is weak and the error for the refractive index is much larger.

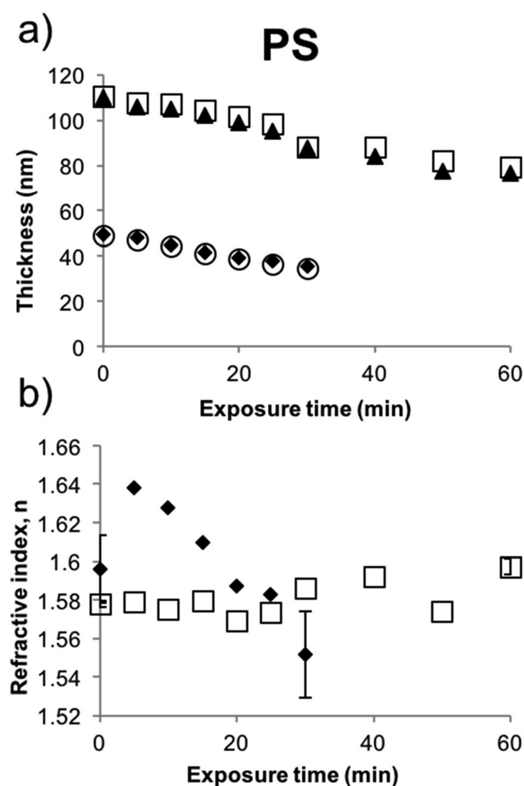

Fig. 4 Effect of UV/air exposure time (min) on PS: (a) thickness (nm) and (b) refractive index values, determined by UV-SR for two samples of PS on SiNx window (on the Si frame) with initial thickness of 49 nm and 110 nm. ○ = thin(t) and ▲ = thick(t) are values where only the thickness was determined using method-ii with k = 0 and fixed refractive index value of 1.587 ± 0.001 at λ = 632.8 nm. ♦ = thin(t,n,k) and □ = thick(t,n,k) are values where both thickness and optical constants were determined using method-i. Note that the larger error bar at the 30 min exposure is because the thickness has decreased to values where the signal is weak and the error for the refractive index is much larger.

each sample, the thickness was determined by both method-i (simultaneously fitting the thickness and the optical constants), and method-ii (using optical constants measured for the non-damaged thick sample). The refractive indices for the non-damaged films at λ = 632.8 nm were 1.482 ± 0.001 for PMMA and 1.587 ± 0.001 for PS, respectively. These values agree with those reported elsewhere.[45]

The UV-SR thickness (determined using both method-i and method-ii) and the refractive index for PMMA (PS) are plotted *versus* the exposure time in Fig. 3a (Fig. 4a) and Fig. 3b (Fig. 4b), respectively. Error bars for the refractive indices are shown for the first (<1 min exposure) and the last (30 min exposure) measurement. After 30 min of exposure the quality of the fit of the $R(\lambda)$ spectrum for the thin PS and PMMA samples decreases and the standard error of the refractive index increases from 0.001 for samples thicker than 50 nm to 0.01 for samples thinner than 50 nm. The measured $R(\lambda)$ spectra for PMMA and PS, which are presented in ESI,† S3, Fig. S2 and S3, change significantly over the 30 min exposure time.

For PMMA, the UV-SR thickness values (Fig. 3a) do not depend on whether method-i or method-ii is used, down to a sample thickness of 25 nm. For PS (Fig. 4a) the two methods produce thicknesses differing by ∼3% for the thick sample. Thicknesses derived using method-ii are systematically lower than those from method-i. PMMA has a rate of thickness decay of 0.97 ± 0.03 and 0.66 ± 0.05 nm min^{-1}, for the thick and thin samples respectively. The rate of thickness decay for the thick PS sample is 0.56 ± 0.04 nm min^{-1}, and 0.48 ± 0.02 nm min^{-1} for the thin PS sample. Thus, relative to PS, PMMA is damaged with lower UV/air exposure. Fig. 3b and 4b show the evolution of the refractive indices with exposure time, as measured using method-i. The refractive index of the PMMA and PS thin films changes by ∼0.1. The error of the refractive index is higher for the thinner samples for both materials. Since the thicknesses derived using method-i and method-ii for the same initial thickness and exposure time are nearly identical (plotted in Fig. 3a and 4a), we conclude that the derived thicknesses are not sensitive to the refractive index changes of ∼0.1 that result from 30 min of UV/air exposure of PS and PMMA.

UV-SR: substrate effect on UV damage of PMMA

From the perspective of the material properties of a polymer film, the derived thickness should not depend on the substrate

 This journal is © the Owner Societies 2018

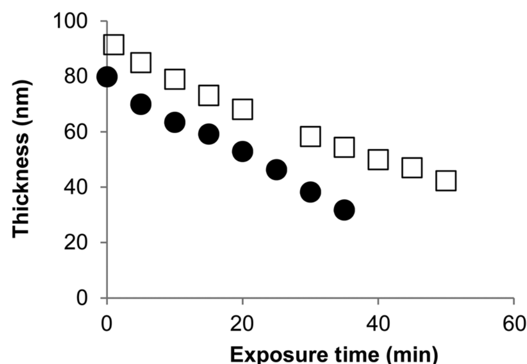

Fig. 5 Influence of substrate on the PMMA thickness dependence of the UV/air exposure, determined using method i. □ = PMMA on 75 nm SiNx on a Si frame, ● = PMMA on a Si wafer with native oxide.

on which the film is deposited. However, if the thin film material partially absorbs radiation then the substrate may affect the degree of absorption because it affects the fraction of light that is reflected from the thin film/substrate interface.[32] Since radiation damage of polymers occurs due to absorption,[28–30] the type of substrate can affect the degree of damage. PMMA was used for this test since it is more sensitive than PS to UV/air damage. Fig. 5 compares the UV-SR thickness as a function of the exposure time measured by method-i, for two substrates: PMMA on SiNx on an oxidized Si wafer and PMMA on an oxidized Si wafer only. The refractive index values determined in these measurements are presented in ESI,† S3 and Fig. S4. Two PMMA samples were used: one film, 91 nm thick before UV damage, was deposited on a 75 nm-SiNx layer on SiO_2 and another film, 80 nm thick before UV damage, was deposited on a clean Si wafer with native oxide. The raw $R(\lambda)$ spectra are shown in ESI,† S3, Fig. S2a and c for PMMA on SiNx on SiO_2, and for the bare Si wafer, respectively. According to Fig. 5, the thickness of the PMMA film on the Si wafer changes more rapidly than that for the PMMA film on SiNx. These results show that the substrate indeed affects the damage rate of UV-sensitive polymers. In particular, using PMMA on the SiO_2 substrate increases the thickness depletion rate by a factor of 2 (slope of Fig. 5), relative to PMMA deposited on SiNx on a SiO_2-on-Si substrate.

STXM: characterization of chemical changes from UV-damage

All of the spectral changes observed in the UV-SR exposed areas are associated with radiation damage caused by UV/air exposure. The regions of the PS, PMMA and PFSA films UV/air exposed to generate the data presented in Fig. 2 were subsequently analyzed by STXM (see Fig. 6–8). A transmission electron microscopy (TEM) Cu grid was placed on top of each polymer film before the UV-SR measurements to shield parts of the sample and produce adjacent sites of exposed and non-exposed sample regions. The TEM grid was removed before the STXM experiments to give access to the non-exposed areas, which were taken as the non-damaged standards for spectroscopic measurements.

For each of Fig. 6–8, image a is an optical image (reflection mode taken with a 15× magnification objective lenses) recorded using the UV-SR microscope with the TEM Cu grid on top of the film; image b is an optical image without the TEM Cu grid, (reflection mode taken with a 50× magnification objective lenses) of the same area after UV-SR measurements; and image c is a STXM image, without the TEM Cu grid, at a photon energy very sensitive to radiation damage. For both PS (Fig. 6b) and PMMA (Fig. 7b), there is a visible discoloration after 30 min UV light exposure and the exposed areas are easily seen in the STXM image. In contrast, PFSA (Fig. 8b) does not show any discoloration after 30 min exposure and the STXM image has uniform signal over the whole UV/SR irradiated area. Table 2 summarizes the thickness of the damaged areas determined by UV-SR after 30 min exposure and by STXM.

STXM: chemical changes of PS films from UV/air damage. The C 1s and O 1s spectra of PS samples UV irradiated in air for 30 min exposure are presented in Fig. 6d and e, while those for 5 min exposure are presented in ESI,† S4 (Fig. S5d and e).

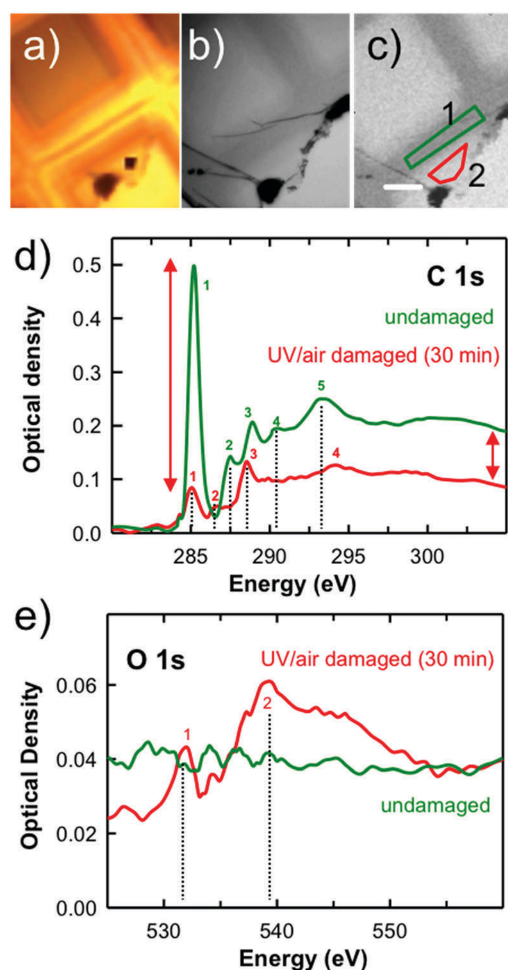

Fig. 6 Optical and STXM characterization of a PS thin film after 30 min of exposure to UV-SR illumination. (a) Visible light image (15×) recorded at the beginning of the measurement. A TEM Cu grid was used as a mask to expose only certain areas and leave others unexposed. (b) Visible light image (50×) of the same area after the UV-SR measurements (the TEM Cu grid has been removed). (c) STXM transmission image at 285.2 eV of the same area. Scale bar is 20 μm. (d) C 1s spectra of the undamaged (green) and strongly damaged (red) areas, indicated in (c). (e) O 1s spectra of the undamaged (green) and damaged (red) areas indicated in (c).

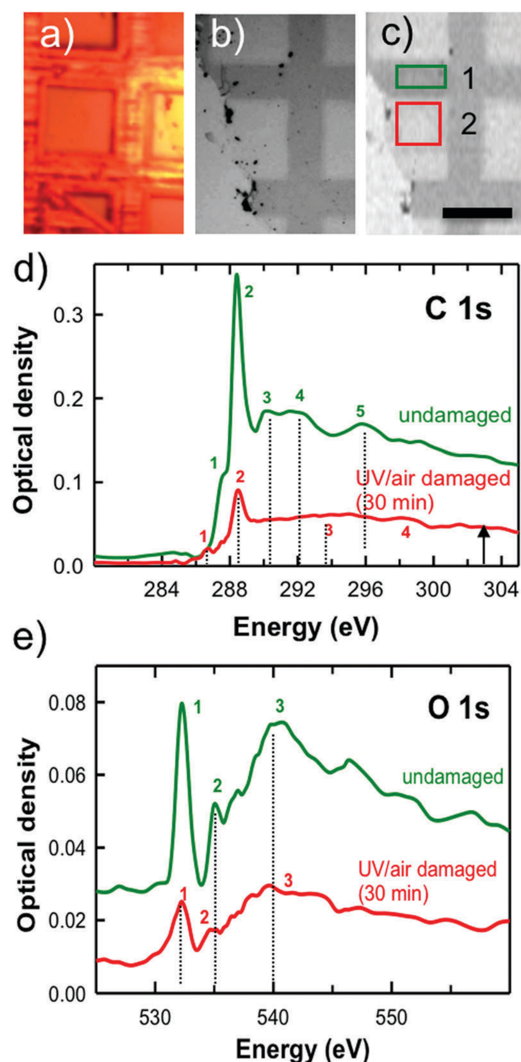

Fig. 7 Characterization of a PMMA thin film after 30 min of exposure to UV-SR illumination. (a) Visible light image (15×) recorded during the measurements. A TEM Cu grid was used as a mask to expose only certain areas and leave others unexposed. (b) Visible light image (50×) of the same area after the UV-SR measurements (TEM grid has been removed). (c) STXM transmission image at 288.4 eV of the same area. Scale bar is 50 μm. (d) C 1s spectra of the damaged (red) and undamaged (green) areas measured at the locations indicated in (c). (e) O 1s spectrum of the damaged (red) and undamaged (green) areas indicated in (c).

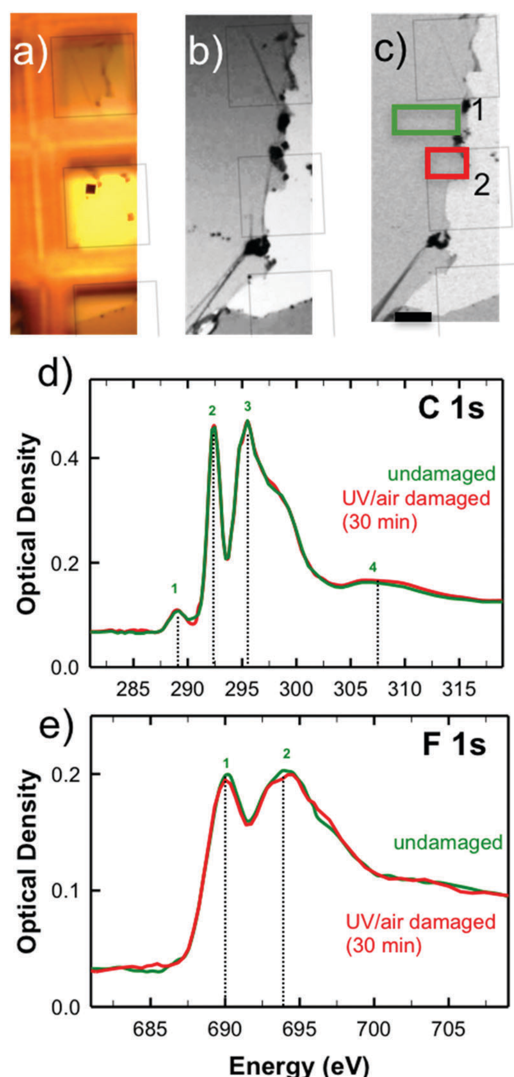

Fig. 8 Characterization of a PFSA thin film after 30 min exposure to UV-SR illumination. (a) Visible light image (15×) recorded during the measurements. A TEM Cu grid was used as a mask to expose only certain areas and leave others unexposed. (b) Visible light image (50×) of the same area after the UV-SR measurements (TEM grid has been removed). (c) STXM transmission image at 690 eV of the same area. Scale bar is 20 μm. The area in the red rectangle is where the PFSA film was UV illuminated while the green rectangle was un-exposed as it was under the TEM grid. (d) STXM C 1s spectrum of the un-exposed (green) and exposed (red) areas (see c). (e) STXM F 1s spectrum of the un-exposed (green) and exposed (red) areas (see c).

Energies and spectral assignments are summarized in Table S1 (ESI,† S4). PS consists of phenyl functional groups attached to an aliphatic main chain (see Scheme 1). The chemical formula of PS is $(C_8H_8)_n$, with monomer molecular mass M_r = 104 g mol^{-1} and a gravimetric density of 1.04 × 10^3 kg m^{-3}. After the 5 min exposure (Fig. S5d, ESI†), there is a small reduction in the intensity of the C 1s → 1$\pi^*_{C=C}$ transition at 285.2 eV (peak 1) while a much larger reduction is observed upon 30 min exposure (Fig. 6d), indicating extensive damage to the phenyl groups. It is also possible that new C═C bonds are formed in the main chain, which would generate signal at 285 eV and partly compensate for phenyl group damage.[25] The C 1s → 2π^* transition present at 287.5 eV[46] (peak 2) in undamaged PS (Fig. 6d) is nearly absent after 30 min UV/air exposure (Fig. 6d), consistent with extensive degradation of the phenyl groups. Also, in the 30 min exposed PS, there is reduced intensity and a shift to higher energy of the peaks at 294 (peak 5 in undamaged → peak 4 in damaged spectrum) and 301 eV which are C 1s(ring) → $\sigma^*_{C=C}$ transitions characteristic of 6-membered unsaturated rings.[46] A new peak appears at 286.6 eV (peak 2 in the damaged spectrum) after 30 min exposure, which corresponds to C 1s(C═O) → $\pi^*_{C=O}$ transitions, indicating that C═O bonds are formed. C 1s (C═O) → $\pi^*_{C=O}$ transitions occur between 286–290 eV for other polymers that have C═O functional groups attached to a chain which also

This journal is © the Owner Societies 2018

Table 2 Thickness (nm) of spin coated films of PS, PMMA and PFSA thin films determined by UV-SR and STXM after 30 min exposure (from Fig. 2 and 6–8)

Material	Thickness (nm)		Ratio UV-SR/ STXM	% difference[d]
	UV-SR ±0.2	STXM		
PS	40.2	35 ± 1[c]	1.15 ± 0.03	12.9 ± 0.4
30 min UV PS[a]	17.5	26.3 ± 0.6	0.67 ± 0.02	−50.3 ± 1.3
PMMA	34.3	30.9 ± 0.6[c]	1.11 ± 0.02	9.9 ± 0.2
30 min UV PMMA[b]	18.2	12.8 ± 0.4	1.42 ± 0.05	29.7 ± 1.0
PFSA	52.0	51.9 ± 0.5[c]	1.00 ± 0.01	0.19 ± 0.00
30 min UV PFSA	51.9	51.3 ± 0.6	1.01 ± 0.01	1.16 ± 0.01

[a] Based on derived chemical formula of $C_8O_4H_8$ for 30 min UV/air damaged PS. [b] Utilized derived chemical formula of $C_5O_4H_8$ for PMMA. [c] STXM thickness determined in adjacent area. [d] Percentage calculated by as (1 − STXM/UV-SR) × 100.

has pendant phenyl groups.[47] Clearly a new chemical species has been formed after 30 min UV/air exposure. In particular, although initially there was very little or no oxygen (Fig. 6e and Fig. S5e, ESI†), an O 1s signal appears even after only 5 min of exposure (Fig. S5e, ESI†), and the O 1s signal increases dramatically with further UV-SR exposure in air. After 30 min, a well-developed O 1s spectrum exists which is dominated by a peak at 531.6 eV (Fig. 6e, peak 1). That peak is the O 1s (C═O) → $\pi^*_{C=O}$ counterpart to the C 1s → $\pi^*_{C=O}$ transition at 286.6 eV (Fig. 6d, peak 2 damaged curve).[48]

The mass loss can be assessed qualitatively from the change in the C 1s continuum intensity. In order to use STXM to determine the thickness of the UV-SR damaged areas a new OD1(E) spectrum was constructed by changing the net-chemical formula to incorporate oxygen (Fig. S6, ESI†). The net-chemical formula accounts for all chemical species absorbing light in the beam cross-section. Initially, there is only PS in the UV-SR irradiated area, but after UV/air damage there is residual PS and the damage product(s). The O-species can be distributed over the film volume or concentrated at the air/film interface. For the 30 min exposed area, the O/C ratio was 0.5, while for undamaged PS the O/C ratio is 0. The changed elemental composition was determined from a simultaneous consideration of the C 1s and O 1s continuum jumps (Fig. S6, ESI†). The appended spectrum was least square fit to match its pre- and post-edge signal to that of the spectrum of a component mass absorption coefficient $\mu_i(E)$ calculated for the net-chemical formula $C_xO_yH_z$. The numbers of C and O atoms ($x_q = x, y$ in ESI,† S2 were chosen to minimize the cumulative residual of the least square fit to the pre- and post-edge regions. The net-chemical formula of UV/air damaged PS was found to be $(C_8O_4H_8)_n$. Using this chemical formula, the C 1s and O 1s OD1(E) reference spectra of UV-damaged PS were obtained from the 30 min exposed sample. Based on this OD1(E) and assuming no change in density, the thickness of the UV damaged area was calculated to be 23 nm, compared to 35 nm of the adjacent pristine (non-damaged) PS (see Table 2), indicating the film thickness decreased by 34% after 30 min UV/air exposure. Note that the intensity of the 285.15 eV $\pi^*_{C=C}$ peak decreases to ~20% of the original intensity after 30 min UV/air exposure whereas about 50% of the carbon remains based on the C 1s continuum intensity at 328 eV (see arrows in Fig. 6d). These results indicate drastic bond re-configuration.

STXM: chemical changes of PMMA films from UV/air damage. The C 1s and O 1s spectra of PMMA samples UV/air irradiated for 30 min are presented in Fig. 7d and e while those for 5 min exposure are presented in ESI,† S4 (Fig. S7d and e, ESI†). Energies and spectral assignments are summarized in Table S2 (ESI,† S4). PMMA has a methyl ester functional group and a methyl group attached to the same carbon of an aliphatic main chain (see Scheme 1). The chemical formula of PMMA is $(C_5O_2H_8)_n$, with a molecular mass M_r = 100 g mol^{-1}, and a gravimetric density of 1.18 × 10^3 kg m^{-3}. The main peak at 288.45 eV is the C 1s(C═O)→ $\pi^*_{O-C=O}$ ester transition (peak 2).[27,47] Its intensity is slightly reduced after 5 min (Fig. S7d, ESI†) and significantly reduced after 30 min UV exposure (Fig. 7d), indicating the ester side chains are removed, probably with production of CO_2, some of which escapes the sample. The C 1s(C–H) → σ^*_{C-H} transition, seen as the small shoulder at 287.6 eV (peak 1 in undamaged spectrum),[47] also decreases in intensity with UV/air exposure. The C 1s(C–C) → σ^*_{C-C} is a broad feature centered around 291.9 eV[47] (peak 4 in undamaged spectrum) that is no longer visible after 30 min exposure (Fig. 7d). A small peak appears at 286.7 eV (peak 1 in damaged spectrum) which could be related to formation of aldehydic C═O bonds. Changes are also observed in the O 1s spectrum (Fig. 7e). The O 1s(C═O) → $\pi^*_{O-C=O}$ peak at 532.3 eV (peak 1), and the O 1s(OCH_3) → $\pi^*_{O-C=O}$ peak[48] at 535.2 eV (peak 2) both decrease (Fig. 7e), consistent with loss of the ester group.[49,50]

After 30 min exposure the C 1s continuum intensity of PMMA decreased by >50% when compared to the adjacent undamaged area, which indicates extensive mass loss and a >50% decrease in thickness. Quantitative thickness analysis with STXM (Table 2) shows that the undamaged PMMA film is 31 nm thick while the damaged PMMA is 11 nm thick (assuming the damaged and un-damaged material have the same density). The new net-chemical formula for the 30 min UV/air radiation damaged area is $C_5O_4H_8$, obtained by the same method used to analyze the composition of the damaged PS, presented above. Fig. S8 (ESI†) presents the simultaneous analysis of the C 1s and O 1s spectra of undamaged and 30 min UV/air damaged PMMA. For the damaged area the O/C elemental ratio was found to be 0.8, while for the non-damaged PMMA area O/C was 0.4. The C 1s and O 1s spectra (Fig. 7e and Fig. S8, ESI†) of the damaged area indicate extensive loss of the ester C═O bonds but the net-chemical formula of $C_5O_4H_8$ indicates an increased O/C ratio (note that both C and O amounts decrease with UV damage). This can be explained by a more rapid loss of C than O. Based on STXM analysis with the estimated formula for the UV damaged PMMA, there is a 65% reduction in thickness in the UV damaged area, relative to the adjacent un-damaged area. This is consistent with results from UV-SR which determined a 50% decrease in thickness (Fig. 3a).

STXM: UV/air does not damage PFSA films. The C 1s and F 1s spectra of the unexposed and the 30 min UV/air exposed areas of PFSA are presented in Fig. 8d and e. Energies and spectral assignments are summarized in Table S3 in ESI,† S4.

The PFSA used in this study has a long side chain, an equivalent weight (EW) of 1100, and a chemical formula of $S_1C_{20}O_5F_{39}H$ with M_r = 1094 g mol^{-1}, and a gravimetric density of 2.00 × 10^3 kg m^{-3}. PFSA consists of a polytetrafluoroethylene (PTFE) backbone with perfluorinated, sulfonate-terminated side chains containing CF, CF_2, CF_3, ether (–O–) and sulfonic acid groups (see Scheme 1). The interpretation of the C 1s and F 1s spectra of PFSA[51] are similar to those of polytetrafluoroethylene (PTFE) and polyvinyldifluoride (PVDF).[52] The strongest C 1s peaks at 292.4 eV and 295.5 eV (peaks 2 and 3 in the C 1s edge) and F 1s peaks at 689.9 eV and 693.9 eV (peaks 1 and 2 in the F 1s edge) are due to 1s → $\sigma^*_{C-F\perp}$ and 1s → $\sigma^*_{C-F\parallel}$ transitions respectively, where the indicated orientation of the upper level is relative to the main polymer chain direction.[51] These transitions are particularly sensitive to ionizing radiation, undergoing damage and mass loss/thickness decrease.[43]

Surprisingly, a 30 min UV/air exposure had no effect on thickness (Table 2), optical response (Fig. S9, ESI†), or the C 1s or F 1s spectra of PFSA (Fig. 8). After UV exposure, there is no change to the C 1s and F 1s spectra when compared to adjacent undamaged areas, consistent with the same thickness of the two regions within the experimental error (51 and 52 nm, respectively, determined from STXM – see Table 2). The raw UV-SR data for exposures of PFSA up to 30 min is shown in Fig. S9 (ESI†). The spectra for all exposure times up to 30 min are identical, consistent with the thickness not changing with UV-SR exposure time. We speculate that the lack of damage when PFSA is UV/air irradiated is the result of negligible UV absorption by PFSA in the 250–400 nm range.[53] In principle, PFSA does absorb UV light in the 200–250 nm range[53] which the UV lamp in the Filmetrics UV-40 unit supplies, but it does not reach the sample due to the ~250 nm low wavelength cutoff of the fiber optic transport system.

Correlating UV-SR and STXM thickness measurements

Thickness measurements were performed on freshly prepared spin coated samples of PS, PMMA and PFSA of at least two different thicknesses. Several areas in each sample (with only underlying SiNx) were either first measured with UV-SR and then STXM, or *vice versa*. A single UV-SR thickness measurement took no longer than 5 s total exposure for all operations. UV-SR measurements were taken from 1–3 adjacent points. STXM was recorded from areas of ~40 μm × 40 μm, which included the same area where the low-dose UV-SR data was measured (see Fig. S1, ESI†). A defocused beam spot (> 0.5 μm) and no-damage conditions were used. The thicknesses determined by UV-SR and STXM for each sample are plotted against each other in Fig. 9 with numerical values listed in Table 3. Linear correlation analysis of this data is presented in ESI,† S5 (Fig. S10 and Table S4). For all film thicknesses, there is an excellent linear correlation of the sample thickness determined by the two methods (R^2 = 0.997, 1.00, 1.00 for PS, PMMA, PFSA respectively). However, the UV-SR thickness values for samples thicker than 100 nm are systematically higher than the STXM determined values (see Fig. 9). The average difference of thicknesses for all 3 materials determined by the two techniques is 10%. For PFSA, the average difference of thicknesses

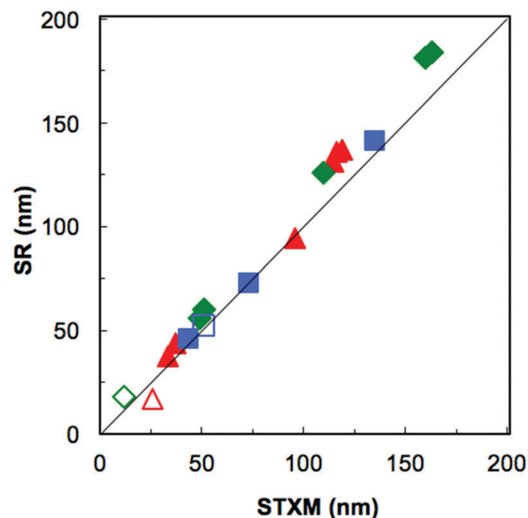

Fig. 9 Plot of thickness of PS, PMMA, and PFSA thin films (both undamaged and UV/air damaged) determined by UV-SR *versus* those derived from STXM. Table 3 lists numerical values. Thicknesses of the UV/air exposed areas from Fig. 2 are the damaged areas. These values were determined by UV-SR before and after exposure, and by STXM from adjacent non-damaged and the UV/air damaged areas. All closed symbols represent undamaged materials, while open symbols represent the UV/air 30 min exposed areas. Undamaged: ▲ = PS, ◆ = PMMA, and ■ = PFSA. UV/air 30 min exposed: △ = PS, ◇ = PMMA, □ = PFSA.

is only 2.8% (which is within 1 standard deviation), while for PS and PMMA the average difference is 11% and 13%, respectively, which is approximately 2 standard deviations. If STXM measurements were done before UV-SR, or *vice versa*, the results were the same.

Thicknesses determined by STXM and UV-SR for the 30 min UV/air damaged samples of PS, PMMA and PFSA in Fig. 6–8 are also plotted in Fig. 9 and listed in Table 3. The difference between STXM and UV-SR thickness values for UV/air damaged PS (53%) and PMMA (33%) is much larger than for the minimal exposure measurements. These differences may be related to density changes in the modified material and uncertainty of the new chemical composition. When plotted against the minimal exposure measurements, the correlated thicknesses of the UV damaged areas are consistent with the general trend of a linear relationship between all of the UV-SR and STXM measurements.

Discussion

Film thickness determination and evolution with UV/air exposure time

When measured under negligible damage conditions, the film thicknesses measured by UV-SR and STXM differ by less than 15% for PS and PMMA and less than 5% for PFSA. The differences between the two methods are not large. In particular, less than 5% systematic difference for PFSA justifies the use of STXM to measure the effective thickness of PFSA ionomer in dispersed CL electrodes for fuel cell applications and supports the use of STXM as a method for quantitative mapping of ionomer distributions in CLs.[1,2] When radiation damage from UV is significant, film

This journal is © the Owner Societies 2018

Table 3 Thickness (nm) of spin coated films of PS, PMMA and PFSA thin films determined by UV-SR and STXM using optimized, low-damage conditions

Material[a,b,c]	Thickness (nm) UV-SR ± 0.2	STXM ± 0.5	Ratio UV-SR/STXM	% difference[d]
PS 1% A	43.7	37.2	1.17 ± 0.02	14.9 ± 0.2
PS 1% B	37.6	33.5	1.12 ± 0.02	10.9 ± 0.2
PS 2%*	94.6	95.5	0.99 ± 0.01	−1.00 ± 0.01
PS 2.6% A*	131	114.7	1.14 ± 0.01	12.4 ± 0.1
PS 2.6% B*	137	118.8	1.15 ± 0.01	13.3 ± 0.1
PS 2.6% C*	136	116.3	1.17 ± 0.01	14.5 ± 0.1
PMMA 2% A	59.9	51.1	1.17 ± 0.01	14.7 ± 0.2
PMMA 2% B	56.1	48.9	1.15 ± 0.01	12.8 ± 0.1
PMMA 3%*	126	110	1.15 ± 0.01	12.7 ± 0.1
PMMA 4% A	184	163	1.129 ± 0.004	11.40 ± 0.04
PMMA 4% B	181	160	1.131 ± 0.004	11.60 ± 0.04
PFSA 4%	141	135	1.044 ± 0.004	4.30 ± 0.02
PFSA 2% A	72.6	73.2	0.99 ± 0.01	−0.80 ± 0.01
PFSA 2% B	45.9	43.6	1.05 ± 0.01	5.0 ± 0.1

[a] Percentage is weight % of the toluene (PS, PMMA) or IPA (PFSA) solution used for spin coating the sample. [b] * indicates STXM measurements were performed first and then UV-SR. [c] A, B, C indicate different regions of the same sample. [d] Percentage calculated as (1 − STXM/UV-SR) × 100.

thickness is reduced and the chemical structure is modified. UV/air and soft X-ray/He (STXM) irradiation affect the sample differently due to the different environmental conditions, and possibly different nature of the applied radiation. All STXM measurements were made in a He atmosphere at ~0.2 atm. It is well known that high doses of soft X-ray cause extensive damage to PMMA[25–27,54] and PFSA.[43] In contrast, PS requires much larger X-ray doses (>10× higher than that for PMMA) for detectible radiation damage.[25] The Filmetrics UV-SR instrument does not provide a means to exclude air from the intersection of the light beam and the sample and so all UV-SR measurements were made in air at 1 atmosphere pressure.

Exposing a polymer film to UV radiation in air induces photochemical reactions in the bulk of the material and at the air/film interface. The change in PS and PMMA sample thickness with UV/air exposure (Fig. 3–5 and Fig. S10, ESI† which combines all the above) can be described by a thickness depletion rate R:

$$\mathrm{d}h(t)/\mathrm{d}t = R, \text{ where } R < 0 \quad (4)$$

Assuming the rate is proportional to thickness, $R = -h(t)b$, where b is a constant independent on time. The differential eqn (4) has the following solution:

$$h(t) = h_0 \mathrm{e}^{-bt}, \text{ were } h_0 = h(t = 0) \quad (5)$$

where $h(t)$ is the time dependent film thickness, t is time and b is reciprocal time $\tau = 1/b$, where τ has a meaning of a characteristic time of the decay. The experimental data presented in Fig. 1 and 3–5 for both PS and PMMA are plotted in Fig. 10 with new dimensionless coordinates $X = tb$ and $Y = \ln(h(t)/h_0)$, where the coefficients h_0 and b were found for each given data set by applying a least square fit with respect to the solution (5), see ESI,† S6 and the Table S5. The points for PS and PMMA

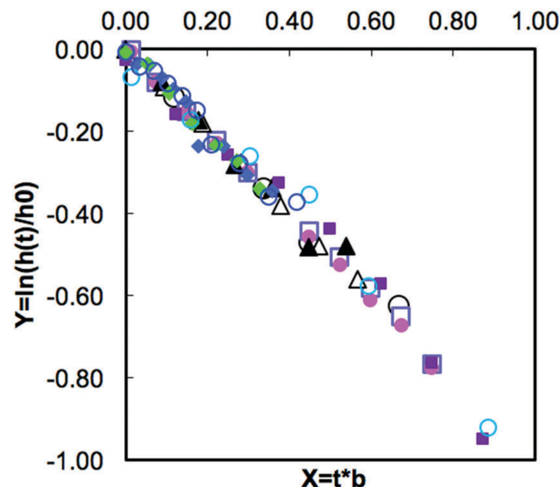

Fig. 10 Plot of thicknesses determined by UV-SR using method-i and ii as a function of UV/air exposure using reduced co-ordinates. See text for details. All closed symbols represent PS, and open symbols represent PMMA. Initial thickness determined by UV-SR: ○ = method-ii PS 110 nm (Fig. 4), ○ = method-ii PS 40 nm (Fig. 2), ◆ = method-i PS 49 nm (Fig. 4), ◆ = method-i PS 110 nm (Fig. 4), ○ = method-ii PMMA 34 nm (Fig. 2), □ = method-ii PMMA 92 nm (Fig. 3), ● = method-i PMMA 91 nm (Fig. 3), Δ = method-ii PMMA 49 nm (Fig. 3), ▲ = method-i PMMA 49 nm (Fig. 3), ■ = method-i PMMA (Fig. 5).

materials collapse along one line with insignificant spread, indicating that dynamic eqn (4) describes the mechanism of the thickness decay and its solution (5) is indeed a reasonable approximation of the thickness evolution measured experimentally. Note, this spread does not reflect measurement uncertainties, which are smaller than the size of each symbol.

Our experiments show that b is between ~0.006 and ~0.03, *i.e.* it is a small parameter, $b \ll 1$, and thus, the solution (5) can be simplified to the linear form (see ESI,† Section 6.II):

$$h(t) \approx h_0(1 - bt) = h_0 - at \quad (6)$$

where parameter $a = h_0 b = h_0/\tau$ is a characteristic rate of the thickness decay. Solution (6) is convenient for analysis the mechanics of the material release from the polymer film due to chemical damage.

Whatever chemical reactions occur upon UV/air irradiation, the damage products must escape through the air/film interface in order to change the film thickness. Those mobile species are most likely of low molecular weight. Two possibilities are considered: (a) the reaction products are released at the air/film interface and all damage processes happen in a thin δ layer near the film surface; (b) the radiation damage products are generated through the bulk of the whole film, migrate to the air/film interface, and then leave the film. Case (a) is limited by the product release rate and is constant for any film thickness. Case (b) is limited by the diffusion of the product(s) through the film and depends on the film thickness.

Thorough testing of both models requires mathematical modeling of the chemical reactions on a microscopic level and is not the target for this paper. However, both mechanisms have been explored as a means to describe the experimentally

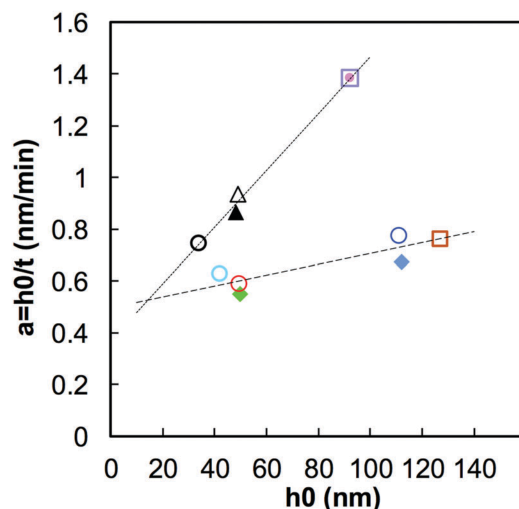

Fig. 11 Rate of reduction of thickness as a function of the initial film thickness for PMMA and PS samples. See text and ESI,† Section 6 for further details. The following samples are on SiNx on SiO_2 frame: ○ = method-ii PS 110 nm (Fig. 4), ○ = method-ii PS 40 nm (Fig. 2), ◆ = method-i PS 49 nm (Fig. 4), ◆ = method-i PS 110 nm (Fig. 4), ○ = method-ii PMMA 34 nm (Fig. 2), □ = method-ii PMMA 92 nm (Fig. 3), ● = method-i PMMA 91 nm (Fig. 3), Δ = method-ii PMMA 49 nm (Fig. 3), ▲= method-i PMMA 49 nm (Fig. 3), ■ = method-i PMMA (Fig. 5).

observed characteristic thickness decay rate a in terms of an initial thickness of the film h_0 and characteristic decay time τ (or $1/b$). The results of this analysis are presented in ESI,† S6, in particular Table S5. Fig. 11 plots a *versus* the initial film thickness h_0 for all PS and PMMA data. Despite having a similar thickness evolution with exposure time $h(t)$ (as shown in Fig. 10), the thickness decay rate a for PS and PMMA depends on the initial film thickness. The decay rate constant for PS films is much less dependent on initial thickness and thus may be limited mostly by surface product release, model (a). The higher dependence on initial film thickness in the case of PMMA suggests there is a larger contribution of bulk diffusion, consistent with model (b). A similar behavior has been observed for PMMA etched with laser.[55] It is important to note, that the decay rate a is inversely proportional to the characteristic time τ (compare Fig. 11 and Fig. S13, ESI†), *i.e.* the thickest PMMA sample has a shorter characteristic thickness decay time than PS.

When extrapolating the PS and PMMA data in Fig. 11 and (ESI† S6, Fig. S13) to $h_0 = 0$, the initial polymer thickness decay rate a and the characteristic time τ are not zero and both parameters do not depend on the material, within the accuracy of our measurements and the validity of the approximations. The parameters $a^* = a(h_0 = 0)$ and $\tau^* = \tau(h_0 = 0)$ could be related to the processes occurring at the surface of the film and the release of the chemical products of the UV damage from the film surface since it depends on the products – not on the initial materials. Thus, it is non-specific and it must have some non-zero value of the rate of the material release. Below we estimate the material removal flux q^* corresponding to this non-specific product release from the film surface. The number of molecules removed is $N = qSt$, where S is the surface area from which N molecules are removed over time t. Also $N = m/M_r$, where m is the removed mass, $m = \rho V$ and M_r is the molecular mass of the removed molecules. The removal flux q is simplified to:

$$q = (\rho/M_r) \times (h/t) \quad \text{or} \quad q^* = a^*\rho/M_r \tag{7}$$

This approach disregards the complexity of the photochemical reactions involved and the identity of the low molecular weight damage products. Eqn (7) is defined for the removed mass for all products of damaged PS and PMMA. For the sake of estimation, we assume: $\rho \sim 1$ g cm^{-3} and $M_r \sim 100$ g mol^{-1}, $\rho/M_r \sim 0.2$ molecule nm^{-3}. As estimated from Fig. 11, $a^* \sim 0.4$ nm min^{-1} is the non-specific flux of molecule removal from the film surface, which corresponds to a rate of $q^* \sim 1.3 \times 10^{-3}$ molecule s^{-1} nm^{-2} or 1 molecule leaving from each 1 nm^{+2} of the film surface every $\sim$750 s. For comparison, the highest flux plotted in Fig. 11 corresponds to a removal rate of $\sim 4.7 \times 10^{-3}$ molecule s^{-1} nm^{-2} or 1 molecule nm^{+2} every $\sim$210 s. The above material removal is quite slow and it requires many seconds to remove a single molecule even for the highest observed removal rate. This correlates with the observation that PS and PMMA develop macroscopically noticeable damage only when they are left under the exposure of the sun for many months or years.

The fact that the polymer film has a limiting thickness decay rate a^* which is non-specific (or nearly non-specific) with respect to polymer material/chemistry is not expected from eqn (7) and can't be predicted from the solution (8). Indeed, the effect of UV/air irradiation is material specific. We attribute the non-specific nature of the limiting thickness decay rate (here and after thickness depletion rate) to a common rate of impingement at the film surface of molecules sufficiently energetic to desorb the low molecular weight UV damage products. Following ref. 56, we estimate the impingement rate of any type of molecule at 1 atmosphere pressure as $\sim 10^9$–10^{10} molecule s^{-1} nm^{-2}. Comparing this with $\sim 10^{-3}$ molecule s^{-1} nm^{-2} removed molecules from the surface we conclude that only a small fraction of the damage products have enough kinetic energy to leave the surface.

Chemistry of UV/air radiation damage

UV photons must be absorbed in order to cause chemical changes. The probability of absorption will in turn depend on the photon energy. The subsequent generation of low molecular weight damage products or radicals[30] will depend on both the net absorption and a complex set of secondary reactions, probably involving electrons, ions and radicals. In order to remove material and thus result in thickness reduction, the damage products must have sufficient kinetic energy to reach and escape from the polymer surface. One effective energy source for material removal could be collisions of energetic gas molecules with the polymer surface. In that case, the molecular mass of the damage product could be a limiting factor: if it is high, or if the radiation-modified species is still attached to the polymer backbone, then thickness erosion will not occur.

The energy range of the light used in UV-SR that is most likely to damage polymers is from 250 nm (4.95 eV) to 400 nm

This journal is © the Owner Societies 2018

(3.10 eV). Transitions $\pi \rightarrow \pi^*$ and $n \rightarrow \pi^*$ associated with specific C═C or C═O bonds occur in this region.[57] Exciting the C═C bonds in PS by using UV-SR in air yields a completely different chemical transformation compared to using 285.1 eV soft X-rays, which corresponds to the C 1s $\rightarrow \pi^*_{C=C}$ absorption as shown in Wang *et al.*, 2009.[25] Soft X-ray excitation induces only a small reduction of the C 1s $\rightarrow \pi^*_{C=C}$ intensity and does not lead to mass loss.[25] In contrast, UV excitation in air causes noticeable changes of both the π^* peak and continuum intensities (see Fig. 6d). The combination of oxygen from air with UV irradiation causes significant damage to the PS, with a high rate of C═C bond dissociation, a reduced C 1s continuum intensity due to mass loss, and clear proof of the formation of C═O bonds (peaks at 288.5 and 539 eV – see Fig. 6b and e). This discrepancy is due to the presence of oxygen in UV-SR which significantly modifies radiation damage of PS, changing both the extent of mass loss and the nature of the chemical changes. A similar effect of oxygen on soft X-ray damage has been noted by Coffey *et al.*[26]

Here we note some remarkable alignments among results of (i) our UV/air measurements and (ii) UV-O plasma treated PS, where the changes were studied by NEXAFS.[58] In the latter work, ozone generated in the plasma significantly accelerates PS radiation damage. The $\pi^*_{C=C}$ signals are reduced, and $\pi^*_{C=O}$ signals are generated.[58] Therefore, we assume that UV/air exposure in the Filmetrics instrument produces ozone in close proximity to the polymer/air interface.

On the other hand, soft X-rays in vacuum rapidly damage PMMA causing destruction of the C 1s $\rightarrow \pi^*_{C=O}$ bonds, thickness decay (net loss of material), and formation of C 1s $\rightarrow \pi^*_{C=C}$ bonds.[25,26] Air or active oxygen species such as ozone are not needed to cause soft X-ray radiation damage to PMMA since oxygen radicals can be generated from the oxygen in PMMA. UV/air irradiation of PMMA also causes substantial damage, which is probably due to an ozonolysis mechanism. Comparing the NEXAFS spectra of the undamaged and UV/air damaged PMMA (Fig. 7) to those reported by Wang *et al.*[25] using soft X-rays at 300 eV, the C 1s $\rightarrow \pi^*_{C=O}$ peak at 288.45 eV is still present in soft X-ray damaged PMMA despite severe mass loss. The shapes of the C 1s and O 1s spectra of damaged and undamaged PMMA (Fig. S7, ESI†) are surprisingly similar, differing mainly in the oxygen composition: $C_5O_{1.3}H_8$ for non-damaged PMMA and $C_5O_{2.5}H_8$ for damaged PMMA. Therefore, oxygen incorporation into damaged PMMA is occurring, probably in a way similar to that of UV/air irradiated PS.

The thickness depletion rates for UV/air irradiated PS and PMMA measured by UV-SR and the major NEXAFS spectral peaks are shown in Fig. 12. For PS, the thickness depletion rate (as measured by UV-SR) is similar to the rate of C═C bond scission, which we define as a ratio of the OD at 285.1 eV (C═C) divided by the OD at 320 eV, represented by the dashed line in Fig. 12a, producing a damage product rich in oxygen (dash-dotted line). The phenyl ring destruction by UV/air exposure corresponds to a process rate-limited by molecule removal at a fixed rate through the surface. For PMMA, the reduction in the $\pi^*_{C=O}$ peak intensity occurs at approximately the same rate as thickness depletion (Fig. 12b). There is a small difference between the thickness depletion rate measured by UV-SR and the rate of reduction of the $\pi^*_{C=O}$ peak intensity in PMMA. This difference can be due to additional structural changes (*i.e.* scissions of C–O and C–C bonds) and diffusion of the radical species that generate damaged products throughout the bulk of the PMMA film.

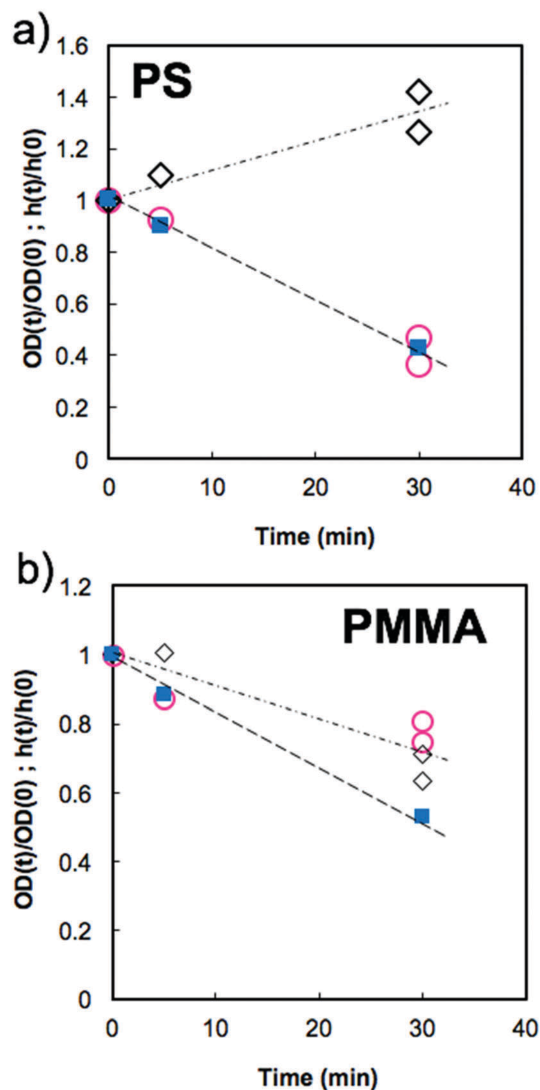

Fig. 12 Thickness measured by UV-SR and NEXAFS spectral feature evolution with time due to UV damage for (a) PS and (b) PMMA. For (a) ○ is the OD at 285.1 eV (C═C) and for (b) the same symbol represents the OD at 288.4 eV (C═O). Both are divided by the OD at 320 eV (total carbon content) of the UV damaged area normalized to the undamaged PS. ◊ is the OD at 538.9 eV divided by the OD at 569 eV (total oxygen content) of the UV damaged area normalized to the undamaged polymer. ■ is the UV-SR thickness for the damaged area normalized to the undamaged polymer. All dashed and dash-dotted lines are qualitative trends for the UV-SR thickness and STXM NEXAFS signals, respectively.

Summary

Two methods of thickness measurements, one based on X-ray absorption, the other based on UV-IR optical interference, were compared. Thicknesses of polymer thin films of PS, PMMA and

PFSA, prepared by spin-coating, were determined using soft X-ray spectromicroscopy (STXM) and the ultraviolet spectral reflectance (UV-SR) methods. It was shown that there is a limit to the allowable UV exposure in air for meaningful results. While it is easy to make single point measurements within the allowable UV exposure, this is not the case for typical mapping applications of the instrument in which many measurements are made at an array of points all within the same UV-illuminated area (500 μm diameter). Since the UV-illuminated area is much larger than the size of the analysis spot (7 μm diameter), a complete map the size of the illuminated area takes 30 minutes or longer, by which time the UV-radiation damage discussed in the paper will have occurred.

When working below the exposure time limit, the chemistry of polymer material is not altered and the average difference between the film thicknesses measured by STXM and UV-SR is below 15% for 30–185 nm thick PS and PMMA films, and $<5\%$ for PFSA films. The observation that polymer film thicknesses derived by UV/SR and STXM are similar is obtained for the first time, providing strong experimental validation of the use of STXM for quantitative determination of ionomer in the cathode layers of PEM-FC.

When long UV/air exposure times were used, the initial chemistry of PS and PMMA films was significantly changed while PFSA films were not affected. Using an exponential depletion model, the rates of PS film depletion could be explained by surface/air interface release of photo-chemical radiation damage products. The higher depletion rates for PMMA suggests a larger contribution of bulk diffusion of the photo-chemical radiation damage products. The depletion rate, a^*, for small thicknesses was found to be similar for both PS and PMMA polymers. A combination of the NEXAFS spectroscopic analysis with the model of thickness depletion and with the results reported in the literature[25,58] suggest that the chemical changes induced by UV/air radiation for PS and PMMA are due to incorporating oxygen from air into the polymer material facilitated by UV generated ozone. We speculate that this effect triggers photo-chemical reactions that significantly damage PS and PMMA. For thickness measurements of polymers sensitive to ozone and oxygen radicals using ultraviolet spectral reflectance (UV-SR) methods, we recommend to blanket the beam-sample area with an inert gas, or to construct a vacuum enclosure.

Conflicts of interest

The authors declare no competing financial interests.

Acknowledgements

The authors acknowledge financial support of AFCC, NSERC (Discovery and CRD grants to APH #RGPIN6141-15), AFCC (purchase of Filmetrics) and the Automotive Partnership Program CaRPE-FC network (stipend and internship support to LM at AFCC, grant # APCPJ417858-11). We thank Menno Bouman at Filmetrics for useful discussions. We thank the beamline scientists at the CLS (Jian Wang) and ALS (David Kilcoyne) for their support of the STXM instruments. The CLS is supported by the Canadian Foundation for Innovation, NSERC, the University of Saskatchewan, the Government of Saskatchewan, Western Economic Diversification Canada, NRC and the Canadian Institutes of Health Research. The ALS is supported by the Director of the Office of Science, Department of Energy, under Contract No. DE-AC02-05CH11231. In addition, we thank the reviewers whose constructive comments resulted in a better understanding of how to model the underlying radiation damage mechanisms.

References

1 D. Susac, V. Berejnov, J. Stumper and A. P. Hitchcock, STXM Characterization of PEM Fuel Cell Catalyst Layers, *ECS Trans.*, 2012, **50**(2), 405–413.
2 D. Susac, V. Berejnov, A. P. Hitchcock and J. Stumper, STXM Study of the Ionomer Distribution in the PEM Fuel Cell Catalyst Layers, *ECS Trans.*, 2011, **41**, 629–635.
3 H. Ade and A. P. Hitchcock, NEXAFS Microscopy and Resonant Scattering: Composition and Orientation Probed in Real and Reciprocal Space, *Polym. J.*, 2008, **49**(3), 643–675.
4 I. N. Koprinarov, A. P. Hitchcock, C. T. McCrory and R. F. Childs, Quantitative Mapping of Structured Polymeric Systems Using Singular Value Decomposition Analysis of Soft X-Ray Images, *J. Phys. Chem. B*, 2002, **106**(21), 5358–5364.
5 C. Ton-That, A. G. Shard and R. H. Bradley, Thickness of Spin-Cast Polymer Thin Films Determined by Angle-Resolved XPS and AFM Tip-Scratch Methods, *Langmuir*, 2000, **16**(5), 2281–2284.
6 R. F. M. Lobo, M. A. Pereira-da-Silva, M. Raposo, R. M. Faria, O. N. Oliveira, M. A. Pereira-da-Silva and R. M. Faria, Thickness Measurements of Ultra-Thin Multilayer Polymer Films By Atomic Force Microscopy, *Nanotechnology*, 2000, **10**, 389–393.
7 E. Tekin, E. Holder, V. Marin, B. J. De Gans and U. S. Schubert, Ink-Jet Printing of Luminescent Ruthenium- and Iridium-Containing Polymers for Applications in Light-Emitting Devices, *Macromol. Rapid Commun.*, 2005, **26**(4), 293–297.
8 Y. Fainman, E. Lenz and J. Shamir, Optical Profilometer: A New Method for High Sensitivity and Wide Dynamic Range, *Appl. Opt.*, 1982, **21**(17), 3200–3208.
9 M. Foster, M. Stamm and G. Reiter, X-Ray Reflectometer for Study of Polymer Thin Films and Interfaces, *Vacuum*, 1990, **41**(4–6), 1441–1444.
10 E. Chason and T. M. Mayer, Thin Film and Surface Characterization by Specular X-Ray Reflectivity, *Crit. Rev. Solid State Mater. Sci.*, 1997, **22**, 1–67.
11 K. Vedam, Spectroscopic Ellipsometry: A Historical Overview, *Thin Solid Films*, 1998, **313–314**, 1–9.
12 S. Kohli, C. D. Rithner, P. K. Dorhout, A. M. Dummer and C. S. Menoni, Comparison of Nanometer-Thick Films by x-Ray Reflectivity and Spectroscopic Ellipsometry, *Rev. Sci. Instrum.*, 2005, **76**(2), 10–15.
13 D. E. Aspnes, Spectroscopic Ellipsometry—A Perspective, *J. Vac. Sci. Technol., A*, 2013, **31**(5), 058502.

 This journal is © the Owner Societies 2018

14 E. A. Irene, *A Brief History and State of the Art of Ellipsometry. In Ellipsometry at the Nanoscale*, Springer Berlin Heidelberg, Berlin, Heidelberg, 2013, pp. 1–30.

15 D. Cattelan, C. Eypert, M. Kloul, M. Gaillet, J.-P. Gaston, R. Seitz, A. Shagaleeva and M. Stchakovsky, *Thin Film Applications in Research and Industry Characterized by Spectroscopic Ellipsometry. In Ellipsometry at the Nanoscale*, Springer Berlin Heidelberg, Berlin, Heidelberg, 2013, pp. 629–667.

16 C. M. Stafford, C. Harrison, K. L. Beers, A. Karim, E. J. Amis, M. R. VanLandingham, H. C. Kim, W. Volksen, R. D. Miller and E. E. Simonyi, A Buckling-Based Metrology for Measuring the Elastic Moduli of Polymeric Thin Films, *Nat. Mater.*, 2004, **3**(8), 545–550.

17 M. W. Meyer, V. H. T. Nguyen and E. A. Smith, Scanning Angle Raman Spectroscopy Measurements of Thin Polymer Films for Thickness and Composition Analyses, *Vib. Spectrosc.*, 2013, **65**, 94–100.

18 Y. Berdichevsky, J. Khandurina, A. Guttman and Y. H. Lo, UV/Ozone Modification of Poly(Dimethylsiloxane) Microfluidic Channels, *Sens. Actuators, B*, 2004, **97**(2–3), 402–408.

19 H. Lu, W. Chen and T. P. Russell, Relaxation of Thin Films of Polystyrene Floating on Ionic Liquid Surface, *Macromolecules*, 2009, **42**(22), 9111–9117.

20 L. J. Crawford and N. R. Edmonds, Calculation of Film Thickness for Dip Coated Antireflective Films, *Thin Solid Films*, 2006, **515**, 907–910.

21 A. Zanutta, F. Villa, C. Bertarelli and A. Bianco, Refractive Index Modulation in Polymer Film Doped with Diazo Meldrum's Acid, *Opt. Mater.*, 2016, **58**, 158–163.

22 A. Vital, M. Vayer, T. Tillocher, R. Dussart, M. Boufnichel and C. Sinturel, Morphology Control in Thin Films of PS:PLA Homopolymer Blends by Dip-Coating Deposition, *Appl. Surf. Sci.*, 2017, **393**, 127–133.

23 Filmetrics Inc., Taking the Mystery out of Thin-Film Measurement, 2016.

24 J. Wang, G. A. Botton, M. M. West and A. P. Hitchcock, Quantitative Evaluation of Radiation Damage to Polyethylene Terephthalate by Soft X-Rays and High-Energy Electrons, *J. Phys. Chem. B*, 2009, **113**(7), 1869–1876.

25 J. Wang, C. Morin, L. Li, A. P. Hitchcock, A. Scholl and A. Doran, Radiation Damage in Soft X-Ray Microscopy, *J. Electron Spectrosc. Relat. Phenom.*, 2009, **170**(1–3), 25–36.

26 T. Coffey, S. G. Urquhart and H. Ade, Characterization of the Effects of Soft X-Ray Irradiation on Polymers, *J. Electron Spectrosc. Relat. Phenom.*, 2002, **122**(1), 65–78.

27 T. Beetz and C. Jacobsen, Soft X-Ray Radiation-Damage Studies in PMMA Using a Cryo-STXM, *J. Synchrotron Radiat.*, 2003, **10**(3), 280–283.

28 A. R. Shultz, Degradation of Polymethyl Methacrylate By Ultraviolet Light, *J. Phys. Chem.*, 1961, **65**(6), 967–972.

29 A. Torikai, M. Ohno and K. Fueki, Photodegradation of Poly(Methyl Methacrylate) by Monochromatic Light: Quantum Yield, Effect of Wavelengths, and Light Intensity, *J. Appl. Polym. Sci.*, 1990, **41**(5–6), 1023–1032.

30 E. Yousif and R. Haddad, Photodegradation and Photostabilization of Polymers, Especially Polystyrene: Review, *Springerplus*, 2013, **2**(1), 398.

31 I. Y. Evchuk, R. I. Musii, R. G. Makitra and R. E. Pristanskii, Solubility of Polymethyl Methacrylate in Organic Solvents, *Russ. J. Appl. Chem.*, 2005, **78**(10), 1576–1580.

32 O. S. Heavens, *Optical Properties in Thin Solid Films*, Dover Publications, Inc., New York, NY, 1991.

33 Norcada, X-ray Microscopy Windows Specification Sheet http://www.norcada.com/wp-content/uploads/2013/10/Xray-Window-Specsheet.pdf.

34 A. P. Hitchcock, Soft X-Ray Imaging and Spectromicroscopy, in *Handbook on Nanoscopy*, ed. G. Van Tendeloo, V. D. Dyck and S. J. Pennycook, Wiley-VCH Verlag GmbH & Co. KGaA, 2012, vol. II, pp. 745–791.

35 H. Ade, A. P. Smith, S. Cameron, R. Cieslinski, G. Mitchell, B. Hsiao and E. Rightor, X-Ray Microscopy in Polymer Science: Prospects of a 'New' Imaging Technique, *Polymer*, 1995, **36**(9), 1843–1848.

36 K. V. Kaznatcheev, C. Karunakaran, U. D. Lanke, S. G. Urquhart, M. Obst and A. P. Hitchcock, Soft X-Ray Spectromicroscopy Beamline at the CLS: Commissioning Results, *Nucl. Instrum. Methods Phys. Res., Sect. A*, 2007, **582**(1), 96–99.

37 A. L. D. Kilcoyne, T. Tyliszczak, W. F. Steele, S. Fakra, P. Hitchcock, K. Franck, E. Anderson, B. Harteneck, E. G. Rightor, G. E. Mitchell, A. P. Hitchcock, L. Yang, T. Warwick and H. Ade, Interferometer-Controlled Scanning Transmission X-Ray Microscopes at the Advanced Light Source, *J. Synchrotron Radiat.*, 2003, **10**, 125–136.

38 T. Warwick, K. Franck, J. B. Kortright, G. Meigs, M. Moronne, S. Myneni, E. Rotenberg, S. Seal, W. F. Steele, H. Ade, A. Garcia, S. Cerasari, J. Denlinger, S. Hayakawa, A. P. Hitchcock, T. Tyliszczak, J. Kikuma, E. G. Rightor, H.-J. Shin and B. P. Tonner, A Scanning Transmission X-Ray Microscope for Materials Science Spectromicroscopy at the Advanced Light Source, *Rev. Sci. Instrum.*, 1998, **69**(8), 2964.

39 J. Stöhr, *NEXAFS Spectroscopy*, 1992, vol. 25.

40 B. L. L. Henke, E. M. M. Gullikson and J. C. C. Davis, X-Ray Interactions: Photoabsorption, Scattering, Transmission, and Reflection at E = 50-30,000 EV, Z = 1-92, *At. Data Nucl. Data Tables*, 1993, **54**(2), 181–342.

41 Hitchcock AXis, AXis 2000 is written in Interactive Data Language (IDL). It Is Available Free for Non-Commercial Use from http://Unicorn.Mcmaster.ca/AXis2000.Html, 2016.

42 C. Jacobsen, S. Wirick, G. Flynn and C. Zimba, Soft X-Ray Spectroscopy from Image Sequences with Sub-100 Nm Spatial Resolution, *J. Microsc.*, 2000, **197**(Pt2), 173–184.

43 L. G. D. A. Melo, G. A. Botton and A. P. Hitchcock, Quantification of the Critical Dose for Radiation Damage to Perfluorosulfonic Acid Membranes Using Soft X-Ray Microscopy, *Microsc. Microanal.*, 2015, **21**(1220), 2443–2444.

44 A. Leontowich, *Tunable Focused X-Rays for Patterning and Lithography*, PhD thesis, McMaster University, 2012.

45 A. V. Leontyev, V. I. Kovalev, A. V. Khomich, F. F. Komarov, V. V. Grigoryev and A. S. Kamishan, PMMA and Polystyrene Films Modification under Ion Implantation Studied by Spectroscopic Ellipsometry, *SPIE*, 2003, **5401**(X), 129–135.

46 J. A. Horsley, J. Stöhr, A. P. Hitchcock, D. C. Newbury, A. L. Johnson and F. Sette, Resonances in the K Shell Excitation Spectra of Benzene and Pyridine: Gas Phase, Solid, and Chemisorbed States, *J. Chem. Phys.*, 1985, **83**(12), 6099.
47 O. Dhez, H. Ade and S. G. Urquhart, Calibrated NEXAFS Spectra of Some Common Polymers, *J. Electron Spectrosc. Relat. Phenom.*, 2003, **128**(1), 85–96.
48 S. G. Urquhart and H. Ade, Trends in the Carbonyl Core (C 1s, O 1s) → Pi*C=O Transition in the near-Edge X-Ray Absorption Fine Structure Spectra of Organic Molecules, *J. Phys. Chem. B*, 2002, **106**(34), 8531–8538.
49 C. Wochnowski, M. A. S. Eldin and S. Metev, UV-Laser-Assisted Degradation of Poly(Methyl Methacrylate), *Polym. Degrad. Stab.*, 2005, **89**(2), 252–264.
50 J. O. Choi, Degradation of Poly(Methylmethacrylate) by Deep Ultraviolet, X-Ray, Electron Beam, and Proton Beam Irradiations, *J. Vac. Sci. Technol., B: Microelectron. Nanometer Struct.--Process., Meas., Phenom.*, 1988, **6**(6), 2286.
51 Z. B. Yan, R. Hayes, L. G. A. Melo, G. R. Goward and A. P. Hitchcock, X-Ray Absorption and Solid-State NMR Spectroscopy of Fluorinated Proton Conducting Polymers, *J. Phys. Chem. C*, 2018, **122**(6), 3233–3244.
52 T. Ohta, K. Seki, T. Yokoyama, I. Morisada and K. Edamatsu, Polarized XANES Studies of Oriented Polyethylene and FIuorinated PolyethyIenes, *Phys. Scr.*, 1990, **41**(4), 150–153.
53 S. H. De Almeida and Y. Kawano, Ultraviolet-Visible Spectra Membrane of Nafion, *Eur. Polym. J.*, 1997, **33**(8), 1307–1311.
54 A. F. G. Leontowich, A. P. Hitchcock, T. Tyliszczak, M. Weigand, J. Wang and C. Karunakaran, Accurate Dosimetry in Scanning Transmission X-Ray Microscopes via the Cross-Linking Threshold Dose of Poly(Methyl Methacrylate), *J. Synchrotron Radiat.*, 2012, **19**, 976–987.
55 N. Bityurin, S. Muraviov, A. Alexandrov and A. Malyshev, UV Laser Modifications and Etching of Polymer Films (PMMA) below the Ablation Threshold, *Appl. Surf. Sci.*, 1997, **109**(110), 270–274.
56 *Surface Analysis: The Principal Techniques*, ed. J. C. Vickerman and I. Gilmore, Wiley, 2009.
57 T. L. Cottrell, *The Strengths of Chemical Bonds, Prop. atoms, radicals, Bond*, 2nd edn, 1966, vol. 372(84), pp. 41–53.
58 R. J. Klein, D. A. Fischer and J. L. Lenhart, Systematic Oxidation of Polystyrene by Ultraviolet-Ozone, Characterized by near-Edge X-Ray Absorption Fine Structure and Contact Angle, *Langmuir*, 2008, **24**(15), 8187–8197.

 This journal is © the Owner Societies 2018